Origin of the hump anomalies in the Hall resistance loops of ultrathin $SrRuO_3/SrIrO_3$ multilayers

Lin Yang [1,*] Lena Wysocki [1] Jörg Schöpf,[1] Lei Jin,[2] András Kovács,[2] Felix Gunkel [3] Regina Dittmann,[3] Paul H. M. van Loosdrecht [1] and Ionela Lindfors-Vrejoiu [1,†]

[1]*Institute of Physics II, University of Cologne, 50937 Cologne, Germany*

[2]*Ernst Ruska-Centre for Microscopy and Spectroscopy with Electrons, Forschungszentrum Jülich GmbH, 52425 Jülich, Germany*

[3]*PGI-7, Forschungszentrum Jülich GmbH, 52425 Jülich, Germany*

(Received 21 August 2020; revised 14 October 2020; accepted 15 December 2020; published 11 January 2021)

The proposal that very small Néel skyrmions can form in $SrRuO_3/SrIrO_3$ epitaxial bilayers and that the electric field effect can be used to manipulate these skyrmions in gated devices strongly stimulated the recent research of $SrRuO_3$ heterostructures. A strong interfacial Dzyaloshinskii-Moriya interaction was considered as the driving force for the formation of skyrmions in $SrRuO_3/SrIrO_3$ bilayers. Here, we investigated nominally symmetric heterostructures in which an ultrathin ferromagnetic $SrRuO_3$ layer is sandwiched between large spin-orbit coupling $SrIrO_3$ layers, for which the conditions are not favorable for the emergence of a net interfacial Dzyaloshinskii-Moriya interaction. Previously the formation of skyrmions in the asymmetric $SrRuO_3/SrIrO_3$ bilayers was inferred from anomalous Hall resistance loops showing humplike features that resembled topological Hall effect contributions. Symmetric $SrIrO_3/SrRuO_3/SrIrO_3$ trilayers do not show hump anomalies in the Hall loops. However, the anomalous Hall resistance loops of symmetric multilayers, in which the trilayer is stacked several times, do exhibit the humplike structures, similar to the asymmetric $SrRuO_3/SrIrO_3$ bilayers. The origin of the Hall effect loop anomalies likely resides in unavoidable differences in the electronic and magnetic properties of the individual $SrRuO_3$ layers rather than in the formation of skyrmions.

DOI: 10.1103/PhysRevMaterials.5.014403

I. INTRODUCTION

Topologically protected magnetic whirls, dubbed as magnetic skyrmions, are considered to be ideal candidates for the potential application in future data storage [1]. This primarily derives from their small size and room temperature stability [2–4], low energy consumption [3–7], and topological protection [8–10]. Epitaxial perovskite oxide heterostructures, such as $SrRuO_3/SrIrO_3$, are considered to have strong interfacial Dzyaloshinskii-Moriya interaction (DMI) due to the broken spatial inversion symmetry and the strong spin-orbit coupling in $SrIrO_3$, and it was reported that Néel skyrmions form in these heterostructures [11,12]. The insulating nature of perovskite oxide heterostructures, such as ultrathin $SrRuO_3/SrIrO_3$, makes them promising systems in terms of electric field manipulation as well as the ability to engineer their magnetic properties. Magnetic skyrmions can in principle be observed in real space by magnetic force microscopy (MFM) [13], Lorentz transmission electron microscopy (LTEM) [14], scanning transmission x-ray microscopy (STXM) [3], spin-polarized scanning tunneling microscopy (SP-STM) [15], x-ray magnetic circular dichroism based photoemission electron microscopy (XMCD-PEEM) [16], spin-polarized low energy electron microscopy (SPLEEM) [17], and in reciprocal space by small-angle neutron scattering (SANS) [18] and resonant small-angle x-ray scattering (SAXS) [19]. However, for epitaxial oxide heterostructures, by using these techniques, the direct observation of sub-100 nm size skyrmions and their characterization become extremely challenging. Therefore, the possibility of examining the formation of skyrmions by magnetotransport measurements is very attractive as Hall resistivity investigations are rather easy to perform in any solid state research laboratory. Recently, there were many reports in which the formation of skyrmions was inferred from the observation of humplike anomalies of Hall resistance loops that were attributed to the manifestation of the topological Hall effect (THE). This is the case of quite a few reports related to epitaxial $SrRuO_3$ heterostructures and to bare $SrRuO_3$ thin films [20–22]. Matsuno *et al.* [11] attributed the observation of such features of Hall loops measured for ultrathin ferromagnetic $SrRuO_3$ [thinner than six pseudocubic unit cells (uc)] capped by 2 uc $SrIrO_3$ thick layer to the formation of skyrmions. Many similar publications followed shortly. There were reports of the humplike features observed in Hall resistance loops of a variety of $SrRuO_3$ based samples: $SrRuO_3/SrIrO_3$ multilayers with relatively thick layers (10 uc thick $SrRuO_3$) [23], $BaTiO_3/SrRuO_3$ bilayers [24], $SrRuO_3$ (5 uc)/$SrIrO_3$ (2 uc) in which the iridate layer was the bottom layer on the $SrTiO_3$ substrate [25], $SrRuO_3$ (8 uc)/$BaTiO_3$ (2 uc) bilayers on $SrTiO_3$ [26], $SrIrO_3$ (2 uc)/$SrRuO_3$ (10 uc) bilayers for which MFM experiments were also performed [12], or relatively thick $SrRuO_3$ (3–6 nm) films grown in low oxygen pressure [27]. Different mechanisms for the occurrence of the interfacial DMI were proposed in these papers, adapted to the particular interfaces and sample peculiarities.

However, the interpretation of the observed humps in anomalous Hall effect (AHE) resistance loops as a fingerprint

*yanglin@ph2.uni-koeln.de
†vrejoiu@ph2.uni-koeln.de

of the THE contribution due to skyrmions is currently under debate. Other reports addressed the possible role played by $SrRuO_3$ layer inhomogeneity, such as Ru/O vacancies [28], thickness variations [29–31], crystal structure distortions [26,32], and intermixing [33] in the occurrence of the THE-like features of the AHE loops. This division of opinions concerning the origin of the THE-like structures of the Hall resistance loops calls for a careful analysis and understanding of the electronic and magnetotransport properties of $SrRuO_3$-based heterostructures. We stress that there are no direct measurements of the magnitude of the interfacial DMI in such epitaxial $SrRuO_3$-based heterostructures, but only the theoretical proposal from Ref. [11], which does not however provide any quantitative microscopic description of how the DMI is generated at the $SrIrO_3/SrRuO_3$ interfaces. There exists very little insight in the interfacial DMI at epitaxial oxide interfaces [34], although hints for the existence of an interfacial DMI in $SrIrO_3$ (2 uc)/$SrRuO_3$ (10 uc) bilayers were inferred from the analyses of the magnetic domain wall chirality [12]. We previously studied asymmetric $SrZrO_3/SrRuO_3/SrIrO_3$ and $SrHfO_3/SrRuO_3/SrZrO_3$ multilayers in which we aimed to observe the possible effects of the net interfacial DMI on the magnetotransport properties and magnetic domain formation [35]. However, these $SrRuO_3$ multilayers, with insulating spacers, were magnetically only very weakly coupled [36] and did not permit a conclusive investigation of the magnetic domains by magnetic force microscopy.

Here we deliberately considered $SrIrO_3/SrRuO_3/SrIrO_3$ epitaxial trilayers and multilayers with several repeats of the trilayer, in order to have interfaces as symmetric as possible in this material system. We aimed to eliminate, or at least minimize, the role of interfacial DMI. In a perfectly symmetric ultrathin film heterostructure the interfacial DMI should cancel out. However, for epitaxial interfaces of perovskite oxides (ABO_3), the interfaces are likely to be asymmetric due to the AO/BO_2 stacking imposed by epitaxial growth, due to asymmetric intermixing or different oxygen octahedral rotations (OOR) angles at the upper and lower interface. For example, the strong influence of the type of interface stacking on the physical properties of perovskite oxide heterostructures was recently demonstrated for $SrIrO_3$-$La_{0.7}Sr_{0.3}MnO_3$ bilayers [37]. For our trilayers and multilayers, because A = Sr for both $SrRuO_3$ and $SrIrO_3$, the interfaces are either of the type $SrO/IrO_2//SrO/RuO_2$ or $IrO_2/SrO//RuO_2/SrO$, and from this viewpoint the interfaces are equivalent.

Prior investigations demonstrated that $SrRuO_3$ layers separated by 2 uc thick $SrIrO_3$ nonmagnetic layers are magnetically decoupled [38]. Therefore, the overall conditions in these $SrIrO_3/SrRuO_3/SrIrO_3$ multilayers strongly disfavor the formation of Néel skyrmions. The trilayer $SrIrO_3/SrRuO_3/SrIrO_3$ samples did not exhibit any hump-like anomalies in the Hall effect loops. In contrast, humplike anomalies were observed over a large temperature range in Hall effect loops of nominally symmetric multilayer samples, in which a $SrRuO_3/SrIrO_3$ bilayer was stacked three or six times. The Hall effect loops with hump anomalies can be the result of inhomogeneous magnetic and electronic properties of the $SrRuO_3$ layers in the multilayers. The inhomogeneous properties possibly arise from layer thickness variation, different degree of intermixing of Ir on the Ru site, and oxygen octahedron deformations that can be different for the $SrRuO_3$ layers next to the substrate and for the layers at the top of the multilayer [39].

II. METHOD

A. Sample growth

The heterostructures studied here, $SrIrO_3/[SrRuO_3/SrIrO_3]_m$ ($m = 1, 6$), were grown on $SrTiO_3(001)$ by pulsed-laser deposition (PLD) using a KrF excimer laser ($\lambda = 248$ nm). $SrTiO_3(001)$ single-crystal substrate was used for the deposition after NH_4F-buffered HF etching for 2–2.5 min and annealing at 1000 °C for two hours in air. The oxygen partial pressure and deposition temperature were optimized at 0.133 mbar and 650 °C for the growth of all the layers. The pulse repetition rate of the laser was 5 Hz and 2 Hz for the $SrRuO_3$ layers and $SrIrO_3$ layers, respectively. The growth of each layer was monitored by high oxygen pressure reflective high-energy electron diffraction (RHEED). The thickness of each $SrRuO_3$ layer is nominally 6 uc and the thickness of each $SrIrO_3$ layer is nominally 2 uc (1 uc layer is ∼0.4 nm thick). The samples were cooled in 100–200 mbar oxygen atmosphere from 650 °C down to room temperature with a rate of 10 °C/minute. A multilayer with $m = 3$, $SrIrO_3/[SrRuO_3/SrIrO_3]_3$, was grown in a second RHEED-PLD system (made by SURFACE systems+ technology GmbH und Co. KG), under similar growth conditions, except for a higher laser fluence and target-to-substrate distance. The properties of the sample with $m = 3$, along with the properties of a second trilayer ($m = 1$) reference sample made in this PLD system, are discussed in the Supplemental Material (see Sec. 2 and Sec. 3) [40].

B. Sample characterization

The surface morphology of our samples was characterized by atomic force microscopy (AFM), as shown in the Supplemental Material [40]. The microstructure of the multilayers, in terms of sharpness of the interfaces, layer thickness, and element distribution, was investigated by high-angle annular dark field scanning transmission electron microscopy (HAADF-STEM) of cross section specimens. The distribution of the atomic elements was observed with high resolution energy dispersive x-ray spectroscopy (EDX). Both STEM and EDX were performed using an electron probe aberration corrected FEI Titan 80–200 ChemiSTEM microscope equipped with in-column EDX detectors. Hall effect measurements were carried out in the four-point geometry (van der Pauw), with permutating contacts for antisymmetrization. Hall resistance loops were recorded both with a physical property measurement system (PPMS, Quantum Design Inc.) and with a homemade setup. The home setup enables the simultaneous measurement of transverse Hall resistance and magneto-optical Kerr effect (MOKE). The polar MOKE studies were performed with the magnetic field applied perpendicular to the thin film surface with incoherent light from a Xe lamp. The probe wavelength was chosen individually for each sample to reduce the contributions of optical artifacts, such as interference effects that can be present in heterostructures with ultrathin films of dissimilar oxides. Light of 491–520 nm wavelength was used for the

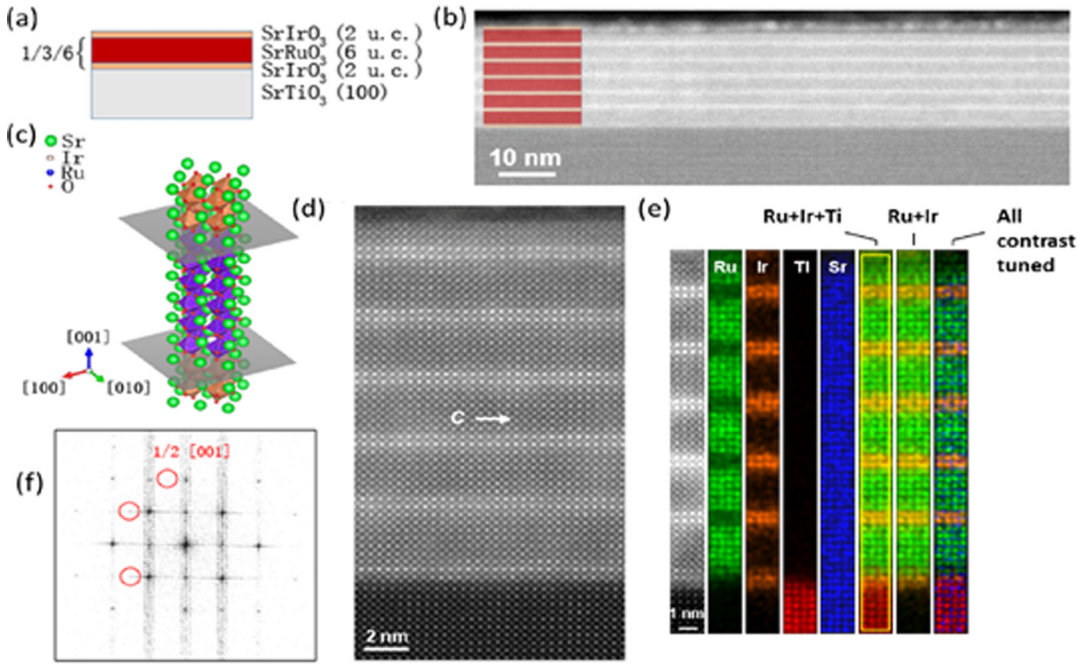

FIG. 1. Microstructure investigations by scanning transmission electron microscopy. (a) Schematics of sample $SrIrO_3/[SrRuO_3/SrIrO_3]_m$ ($m = 1, 3, 6$) grown on $SrTiO_3(100)$ substrates. (b) An overview HAADF-STEM micrograph of sample $SrIrO_3/[SrRuO_3/SrIrO_3]_6$ indicates the layers are uniform (except for the top layer that was damaged during the FIB processing of the specimen). (c) Schematics of the structure of the trilayer $SrIrO_3/[SrRuO_3/SrIrO_3]_1$, for which a 6 uc $SrRuO_3$ layer is inserted between two $SrIrO_3$ layers (both 2 uc thick). Green, orange, blue, and red dots represent Sr, Ir, Ru, and O atomic column positions, respectively, in the crystal structure drawn using VESTA [41]. In (d) and (e) high magnification micrographs show the quality of the interfaces. EDX elemental mapping across the entire stacks shown in (e) probed the uniformity of chemical element distribution. (f) FFT pattern obtained from the image shown in (d), which shows the spots due to the reflections originating from the orthorhombic distortion (marked by red circles), and confirms the in-plane c-axis orientation of the layers [white arrow in (d)].

$SrIrO_3/[SrRuO_3/SrIrO_3]_1$ trilayers, 630 nm wavelength was used for the $SrIrO_3/[SrRuO_3/SrIrO_3]_3$, and 610 nm wavelength was used for the $SrIrO_3/[SrRuO_3/SrIrO_3]_6$ multilayer.

The magnetic moment of the samples was measured as a function of temperature and magnetic field using a superconducting quantum interference device (SQUID) magnetometer (MPMS XL-7 from Quantum Design). The magnetic background due to the diamagnetic $SrTiO_3$ substrates was subtracted from the total magnetic response and often also corrections for a ferromagnetic impurity contribution had to be applied [35].

III. RESULTS AND DISCUSSION

A. Microstructure investigations

The results of microstructure investigations by HAADF-STEM and high-resolution EDX are summarized in Fig. 1. The overall structure of the heterostructures under study here, $SrIrO_3/[SrRuO_3/SrIrO_3]_m$ ($m = 1, 3, 6$) is shown in Fig. 1(a), whereas the symmetric unit cell structure of the repetitive trilayer building block is depicted in Fig. 1(c). Figures 1(b) and 1(d) show cross-sectional STEM images of the microstructure of the $SrIrO_3/[SrRuO_3/SrIrO_3]_6$ multilayer at low and high magnification, respectively. The stacking starts with a $SrIrO_3$ and individual $SrRuO_3$ and $SrIrO_3$ layers have thicknesses that match fairly well the expected thickness values from the *in situ* RHEED monitoring of the layer deposition [see Supplemental Material, Fig. S1(c)] [40]. The high resolution image [Fig. 1(d)] indicates coherent epitaxial growth of the layers, as no dislocations were detected across the entire stack in the investigated TEM specimen. The high resolution EDX mapping of the elements across the entire stacks [Fig. 1(e)] indicates that Ru and Ir are distributed as expected from the designed growth sequence starting with a $SrIrO_3$ layer as the first layer on the substrate. We could not analyze quantitatively the exact stoichiometry of the individual layers. Line profiles confirmed that the $SrRuO_3$ layers are about 6–7 uc thick (as the number of individual Ru-O_2 planes varies between 6 and 7), while the $SrIrO_3$ layers are 2–3 uc thick (as the number of individual Ir-O_2 planes varies between 2 and 3) (see Supplemental Material, Fig. S2) [40]. Concerning the intermixing, because the individual $SrIrO_3$ layers are much too thin, no quantitative analyses of the possible intermixing at the interfaces with the $SrRuO_3$ layers are feasible. Achieving atomic resolution in EDX investigations, due to the electron beam channeling, volume, and spectrum background effects, is very problematic.

The structure was analyzed by fast Fourier transform (FFT) images [Fig. 1(f)] which confirm the in-plane c-axis orientation of the layers (see white arrow) and demonstrate the expected orthorhombic distortions (due to A-site atom displacements of the pseudocubic perovskite ABO_3) by the presence of extra reflections, marked by the red circles in Fig. 1(f).

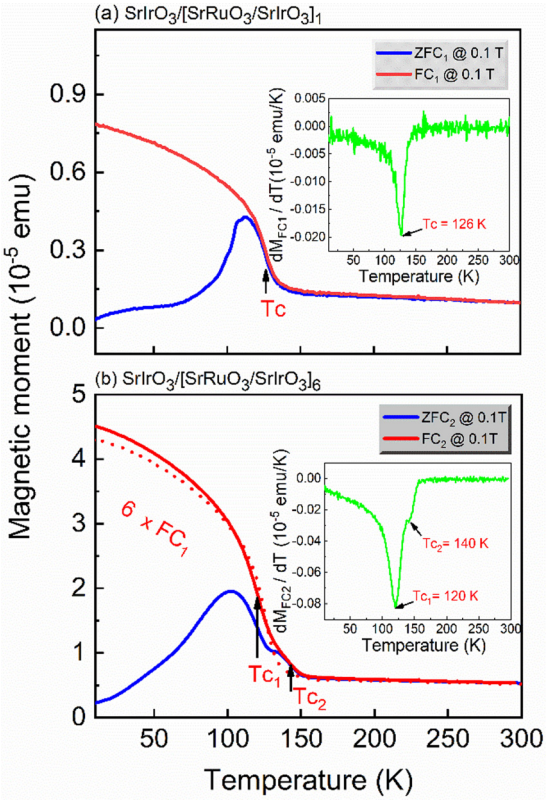

FIG. 2. Temperature dependence of the magnetic moment of the samples (a) $SrIrO_3/[SrRuO_3/SrIrO_3]_1$ and (b) $SrIrO_3/[SrRuO_3/SrIrO_3]_6$ under zero field cooling (ZFC, blue plot) and field cooling (FC, red plot, 0.1 T applied perpendicular to the sample surface) conditions. The dotted red curve shown in (b) is the FC_1 curve of the trilayer sample from (a) multiplied by six and plotted for the sake of comparison. The insets in (a) and (b) show the first derivative of the magnetization with respect to temperature, used to determine the Curie transition temperatures of the $SrRuO_3$ layers.

B. Magnetic properties

We measured the dependence of the out-of-plane total magnetic moment as a function of temperature, under zero-field cooling [ZFC, measured while heating up in 0.1 Tesla (T) after cooling the sample with no applied field] and field cooled (FC) with a 0.1 T field applied perpendicular to the sample surface. The results for the $SrIrO_3/[SrRuO_3/SrIrO_3]_1$ trilayer and the $SrIrO_3/[SrRuO_3/SrIrO_3]_6$ multilayer are summarized in Fig. 2. For the trilayer sample, the Curie temperature (T_c) is 126 K, which was determined from the derivative of the FC magnetic moment curve as a function of temperature [see inset in Fig. 2(a)]. The T_c of the 6 uc thick $SrRuO_3$ layer of this sample is lower than for the bulk $SrRuO_3$ single crystals (T_c = 160 K), which is typical for ultrathin films, due to epitaxial strain and disorder and stoichiometry effects, which are more pronounced the thinner the $SrRuO_3$ layers are [42]. The magnitude of the magnetic moment for $SrIrO_3/[SrRuO_3/SrIrO_3]_6$ is almost six times as large as $SrIrO_3/[SrRuO_3/SrIrO_3]_1$ [see the red dotted curve in Fig. 2(b)], corresponding to the magnetic volume relation of these two samples. Apparently two transitions at temperatures T_{c1} (120 K) and T_{c2} (140 K) occur for the $SrIrO_3/[SrRuO_3/SrIrO_3]_6$ epitaxial multilayers. We assume that the occurrence of two transition temperatures originates from the inhomogeneous magnetic properties of the $SrRuO_3$ layers. Most likely the six $SrRuO_3$ layers of the $SrIrO_3/[SrRuO_3/SrIrO_3]_6$ have all slightly different Curie temperatures distributed in the interval between T_{c1} and T_{c2}. Comparing with the transition temperature of the trilayer sample, which is 126 K, we are led to consider that the bottommost $SrRuO_3$ layer has the lowest Curie temperature, while the top $SrRuO_3$ layers have the largest Curie temperature. It is likely that the bottommost $SrRuO_3$ layers are most affected by the epitaxial strain and oxygen octahedral accommodation to the conditions of the $SrTiO_3$ substrate, resulting in suppressed Curie temperature. The topmost $SrRuO_3$ layers of the multilayer may have structures that are more relaxed towards the bulk $SrRuO_3$ structure, approaching the OOR values of the bulk, and thus have larger Curie temperature.

Two ferromagnetic transition temperatures were reported recently for $(SrRuO_3)_n/(SrIrO_3)_n$ superlattices with ultrathin individual layers ($n \leqslant 3$) [43]. The high temperature transition, occurring also at 140 K as for our samples, was attributed to the interesting possibility that the ultrathin $SrIrO_3$ layers undergo a canting antiferromagnetic transition. This transition vanished for the superlattices with thicker layers, $n \geqslant 4$. As stressed in this reference, no x-ray circular magnetic dichroism spectroscopy (XCMD) measurements at the Ru and Ir edges have been performed yet to test this proposal. There are however XMCD studies of $LaMnO_3/SrIrO_3$ superlattices, which demonstrate the formation of interfacial Ir-Mn molecular orbitals and ferromagnetic order of the Ir magnetic moments [44].

The comparison of the out-of-plane total magnetic moment hysteresis loops, measured with the SQUID magnetometer, and of the MOKE rotation angle loops of the samples with $m = 1$ and $m = 6$ is shown in Fig. 3(a) and Fig. 3(b), respectively. We plotted together the SQUID and MOKE hysteresis loops of the same sample at several temperatures (10 K, 50 K, 80 K). The coercive fields determined by SQUID and MOKE measurements are almost identical. The SQUID and MOKE loops of both samples are in very good agreement except for the regions of saturated magnetization, for relatively high fields. This discrepancy stems from the corrections that had to be applied to both type of loops: The loops are affected by different contributions either from the diamagnetic substrate and ferromagnetic impurities for SQUID loops or from the cryostat window in the case of the MOKE loops. The temperature dependence of the coercive field, extracted from loops measured by SQUID and MOKE, is compared for the two samples in Fig. 3(c). The magnitude of coercive fields and their temperature dependence is in good agreement with results of previous work [36].

C. Anomalous Hall resistance and MOKE hysteresis loops

For the particular samples under study, the measured total Hall voltage has a contribution from the ordinary Hall effect and a contribution from the anomalous Hall effect, at temperatures below the Curie temperature of the $SrRuO_3$ layers. The total Hall voltage V_{yx} was measured in van der Pauw configuration [as shown in the schematic inset of Fig. 4(a)].

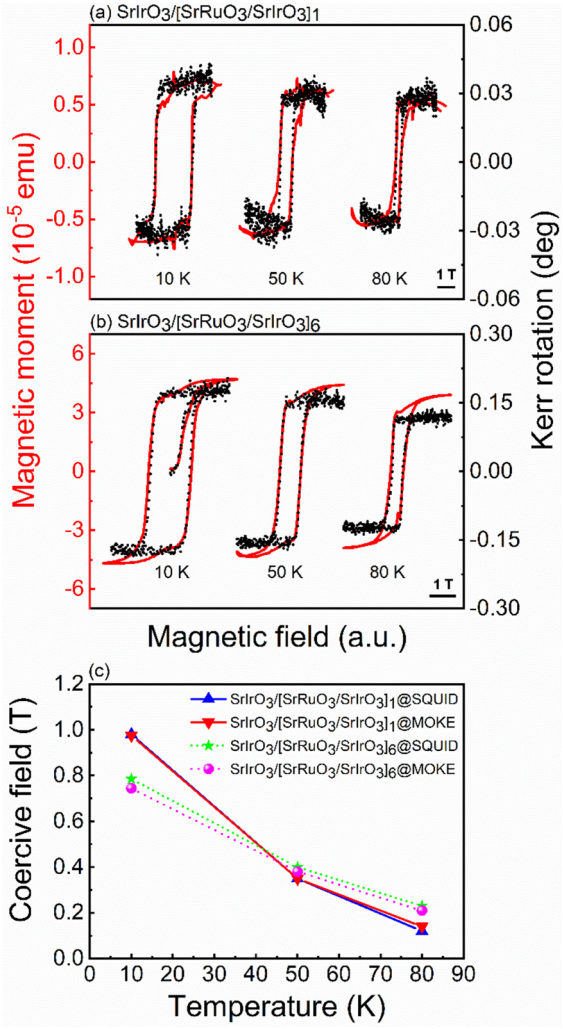

FIG. 3. Magnetic moment hysteresis loops (measured by SQUID magnetometry, red loops) and MOKE rotation angle loops for samples (a) $SrIrO_3/[SrRuO_3/SrIrO_3]_1$ and (b) $SrIrO_3/[SrRuO_3/SrIrO_3]_6$, measured in perpendicular magnetic field. (c) Comparison of the coercive fields of these two samples at different temperatures, as obtained from the SQUID and MOKE hysteresis loops. The lines are guides for the eye.

We define the transverse Hall resistance R_{yx} as the ratio of the Hall voltage and the excitation current I: $R_{yx} = V_{yx}/I$.

For the $SrIrO_3/[SrRuO_3/SrIrO_3]_m$ multilayers, the metallic $SrRuO_3$ layers are magnetically decoupled [36] and are electrically connected in parallel. The $SrRuO_3$ layers have very similar resistances, because they have nominally the same thickness and similar interfaces [45]. The contribution of the ordinary Hall effect to the measured Hall voltage V_{yx} was subtracted from all the Hall loops shown in the paper: We assumed that in the high magnetic field range, when the magnetization of the sample gets saturated, the only field dependence comes from the linear contribution of the ordinary Hall effect. Therefore, in the following R_{yx} reflects the anomalous Hall effect of the samples and we refer to it as the anomalous Hall resistance in discussing the data presented in Fig. 4 and in the Supplemental Material [40].

The hysteresis loops of R_{yx} at fixed temperature in the range 10–110 K/120 K of the $SrIrO_3/[SrRuO_3/SrIrO_3]_1$ and $SrIrO_3/[SrRuO_3/SrIrO_3]_6$ samples are plotted in Fig. 4(a) and Fig. 4(b), respectively. We note that the anomalous Hall resistance of these two samples exhibits a sign change from negative (at low temperatures) to positive around 86 K. This change of sign is typical for $SrRuO_3$ epitaxial films as well as single crystals [46], consistent with previous experimental data and theoretical predictions [11,47–52]. This peculiar sign change, from negative to positive as the temperature increases, comes from the change of the sign of the intrinsic anomalous Hall conductivity. The latter is the result of the presence of Weyl-like nodes, acting as magnetic monopoles, in the electronic band structure of $SrRuO_3$, combined with changes in the band structure as a function of the magnetization (and thus of the temperature). Although the existence of magnetic monopoles in $SrRuO_3$ is not experimentally unambiguously proved yet, the three-dimensional bulk $SrRuO_3$ has been considered as a system for which a large intrinsic AHE driven by topological band structure can be observed [46]. As the energies of nodal points and lines are different, when the Berry curvatures from them have opposite signs, the magnitude and the sign of intrinsic AHE conductivity can be tuned by changing the position of the Fermi level [50,51,53]. We note that measurements of a second trilayer sample, made in another PLD chamber, agree qualitatively with the AHE and MOKE loops data of the trilayer discussed here (see Supplemental Material, Fig. S3 and Fig. S5] [40]. The most important observation is that the trilayer samples do not exhibit any humplike anomalies in the as measured Hall effect loops, as this is expected for symmetric interfaces. In contrast, our asymmetric bilayers with only one $SrRuO_3/SrIrO_3$ interface of the same structural quality as for the trilayers, as studied in our previous work [35,49] (see also comparative AHE loops data for a bilayer in Supplemental Material, Fig. S7) [40], do show humplike features in the vicinity of the temperature at which AHE constant changes sign.

Interestingly, the AHE resistance loops of the multilayer sample ($m = 6$) do show humplike features within a broad temperature range from 70–110 K [see Fig. 4(b)]. These features of Hall resistance loops are peculiar, if compared with the corresponding magnetization/Kerr rotation angle loops measured at the same temperature. For the multilayer, the AHE and MOKE loops at the temperatures where the hump features occur are strikingly different, as obvious in the selected plots in Fig. 4(d). This indicates that the AHE resistance loops of the multilayer do not directly scale with the magnetization loops, as conventionally expected if the AHE constant was the same, in terms of magnitude and temperature dependence, for all six $SrRuO_3$ layers of the multilayer.

We made a symmetric $SrIrO_3/[SrRuO_3/SrIrO_3]_m$ ($m = 3$) multilayer in the second PLD system, with the same PLD parameters as for the second trilayer $SrIrO_3/[SrRuO_3/SrIrO_3]_1$. The AHE and MOKE loops of this multilayer with $m = 3$, at different temperatures, are summarized in the Supplemental Material (see Fig. S4) [40]. The behavior of the AHE loops was very intricate for this particular multilayer and humplike features occur in the temperature range of 10–80 K. We thus confirmed that the multilayers did have in common the appearance of the hump anomalies, in contrast to the bare trilayers.

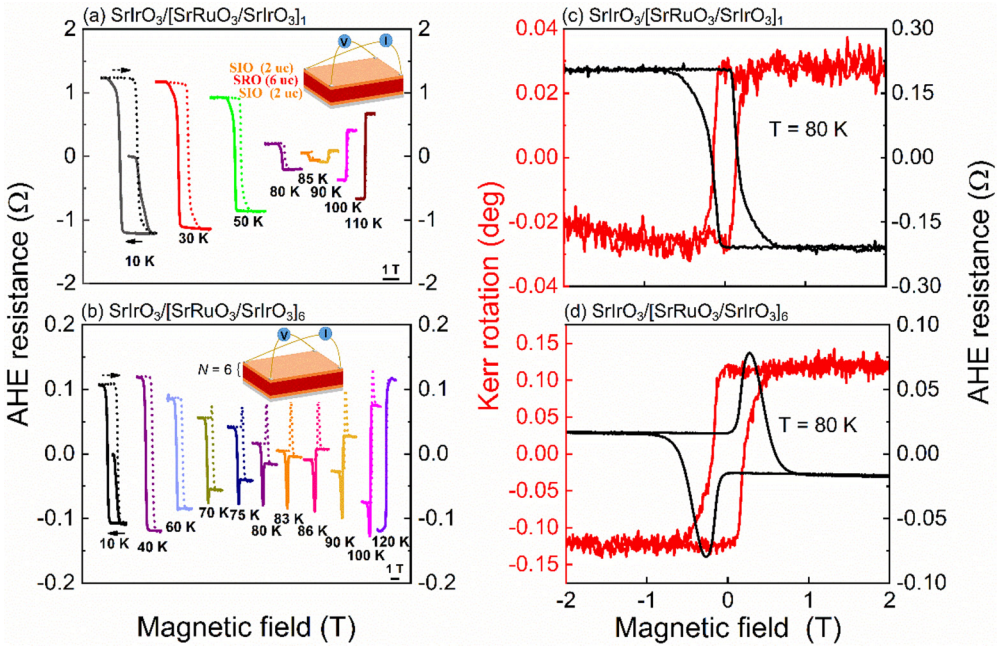

FIG. 4. Summary of the anomalous Hall effect (AHE) resistance R_{yx} loops of the $SrIrO_3/[SrRuO_3/SrIrO_3]_m$ ($m = 1, 6$) samples, as a function of temperature: (a) for $SrIrO_3/[SrRuO_3/SrIrO_3]_1$ and (b) for $SrIrO_3/[SrRuO_3/SrIrO_3]_6$. In (c) and (d) the anomalous Hall resistance loops (black) and the MOKE rotation angle loops (red) measured at 80 K for sample $SrIrO_3/[SrRuO_3/SrIrO_3]_1$ and $SrIrO_3/[SrRuO_3/SrIrO_3]_6$, respectively, are compared.

Our symmetric multilayers, $SrIrO_3/[SrRuO_3/SrIrO_3]_6$ and $SrIrO_3/[SrRuO_3/SrIrO_3]_3$, had a geometry that minimizes a net interfacial DMI. The lack of net DMI is a strong indication that other mechanisms than skyrmions and their topological Hall effect have to be considered for the hump anomalies of the AHE hysteresis loops. A more plausible explanation is that the individual $SrRuO_3$ layers of the multilayer $SrIrO_3/[SrRuO_3/SrIrO_3]_6$ have slightly different magnetic properties (i.e., saturation magnetization, coercive field, T_c), as a result of chemical and structural differences among each other (originating from slight layer thickness variation, different degree of intermixing of Ir on the Ru site, and oxygen octahedron deformations). These differences, though probably minute, are of great importance for the temperature dependence and the magnitude of the intrinsic anomalous Hall resistivity of each layer. Hence, the individual ferromagnetic $SrRuO_3$ layers generate several independent magnetotransport channels leading to the observed hump anomalies of the AHE loops. As proposed in several papers [28,33,53–55] and in our previous reports [32,35,38], the humplike anomalies of the AHE hysteresis loops in $SrRuO_3$-based heterostructure can be well explained by a model of several independent magnetic channels, with distinct coercive fields and different temperatures at which the intrinsic AHE conductivity changes sign.

IV. SUMMARY

In epitaxial asymmetric $SrRuO_3/SrIrO_3$ bilayers a strong interfacial Dzyaloshinskii-Moriya interaction (DMI) was proposed to emerge and to be the driving force for the formation of skyrmions. These skyrmions would result in a topological Hall effect, whose manifestation was considered to be spotted as humplike features, developing while the magnetization of the $SrRuO_3$ layer reversed between saturated states. We studied here heterostructures in which an ultrathin ferromagnetic $SrRuO_3$ layer was sandwiched between $SrIrO_3$ layers. Principally, this geometry disfavors the occurrence of a net interfacial DMI and thus the formation of skyrmions would be exceptional. $SrIrO_3/SrRuO_3/SrIrO_3$ trilayers did not have hump anomalies of the Hall resistance loops. However, the Hall resistance loops of multilayers, in which the trilayer was stacked several times, did exhibit the humplike structures, similar to the asymmetric $SrRuO_3/SrIrO_3$ bilayers. The magnetization as a function of temperature indicated that the multilayers had a spread of the Curie temperatures, hinting to differences in the magnetic properties of the individual $SrRuO_3$ layers. The origin of the Hall effect anomalies likely stems from unavoidable structural differences between the individual $SrRuO_3$ layers stacked in epitaxial multilayers. The minute structural differences (oxygen octahedra rotation angles, bond lengths) of the individual ruthenate layers result in inhomogeneous magnetic and electrical properties across the multilayer. It is possible that the individual $SrRuO_3$ layers generate several independent magnetotransport channels leading to the observed anomalous features of the Hall effect loops. The possibility that the hump anomalies have a relation to the skyrmion formation cannot be ruled out, however our data strongly support the interpretation in terms of multiple magnetotransport channels present in multilayers. We stress that to the best of our knowledge there is no experimental evidence of the existence of DMI at the epitaxial interface of the ferromagnetic $SrRuO_3$ and of the large spin-orbit coupling $SrIrO_3$ and the interfacial DMI is still only at the level of speculative assumption. Experiments of Brillouin light scattering (BLS) [56,57], which are routinely employed for determin-

ing the strength and sign of interfacial DMI, but chiefly for systems that are magnetically ordered at room temperature, are rarely performed at low temperatures, such as needed for $SrRuO_3/SrIrO_3$. No BLS investigations have been reported so far on epitaxial all-oxide heterostructures. Focused studies must be dedicated to the essential aspect of DMI determination, from both theoretical and experimental viewpoints, starting with the understanding of the microscopic mechanism of DMI at epitaxial all-oxide interfaces.

ACKNOWLEDGMENTS

We thank Michael Ziese for constant valuable advice with the physical properties of $SrRuO_3$ samples and with the SQUID and Hall measurements (University of Leipzig). We are grateful to Achim Rosch for fruitful discussions and insightful suggestions, Susanne Heijligen for kind assistance with SQUID measurements, and Andrea Bliesener for AFM and assistance with the PPMS measurements (University of Cologne). We thank René Borowski for etching the STO substrates (FZ Julich). This work was supported by the Deutsche Forschungsgemeinschaft (DFG) (project numbers 335038432 and 403504808) and through CRC1238 (Project No. 277146847). P.H.M.v.L. and I.L.-V. thank DFG for funding the purchase of the PLD-RHEED system at University of Cologne, with which some of the investigated samples were grown (Project No. 407456390). Also support from the German Excellence Initiative via the key profile area "quantum matter and materials" (QM2) of the University of Cologne is gratefully acknowledged. L.Y. thanks the financial support from the China Scholarship Council (File No. 201706750015).

[1] N. S. Kiselev, A. N. Bogdanov, R. Schäfer, and U. K. Rößler, Chiral skyrmions in thin magnetic films: New objects for magnetic storage technologies? J. Phys. D **44**, 392001 (2011).

[2] A. Soumyanarayanan, M. Raju, A. L. G. Oyarce, A. K. C. Tan, M.-Y. Im, A. P. Petrović, P. Ho, K. H. Khoo, M. Tran, C. K. Gan, F. Ernult, and C. Panagopoulos, Tunable room-temperature magnetic skyrmions in Ir/Fe/Co/Pt multilayers, Nat. Mater. **16**, 898 (2017).

[3] S. Woo, K. Litzius, B. Krüger, M.-Y. Im, L. Caretta, K. Richter, M. Mann, A. Krone, R. M. Reeve, M. Weigand, P. Agrawal, I. Lemesh, M.-A. Mawass, P. Fischer, M. Kläui, and G. S. D. Beach, Observation of room-temperature magnetic skyrmions and their current-driven dynamics in ultrathin metallic ferromagnets, Nat. Mater. **15**, 501 (2016).

[4] S. Das, Y. L. Tang, Z. Hong, M. A. P. Gonçalves, M. R. McCarter, C. Klewe, K. X. Nguyen, F. Gómez-Ortiz, P. Shafer, E. Arenholz, V. A. Stoica, S.-L. Hsu, B. Wang, C. Ophus, J. F. Liu, C. T. Nelson, S. Saremi, B. Prasad, A. B. Mei, D. G. Schlom, J. Íñiguez, P. García-Fernández, D. A. Muller, L. Q. Chen, J. Junquera, L. W. Martin, and R. Ramesh, Observation of room-temperature polar skyrmions, Nature (London) **568**, 368 (2019).

[5] X. Z. Yu, N. Kanazawa, W. Z. Zhang, T. Nagai, T. Hara, K. Kimoto, Y. Matsui, Y. Onose, and Y. Tokura, Skyrmion flow near room temperature in an ultralow current density, Nat. Commun. **3**, 988 (2012).

[6] A. Fert, V. Cros, and J. Sampaio, Skyrmions on the track, Nat. Nanotechnol. **8**, 152 (2013).

[7] J. Iwasaki, M. Mochizuki, and N. Nagaosa, Universal current-velocity relation of skyrmion motion in chiral magnets, Nat. Commun. **4**, 1463 (2013).

[8] C. Reichhardt, D. Ray, and C. J. Olson Reichhardt, Collective Transport Properties of Driven Skyrmions with Random Disorder, Phys. Rev. Lett. **114**, 217202 (2015).

[9] W. Jiang, P. Upadhyaya, W. Zhang, G. Yu, M. B. Jungfleisch, F. Y. Fradin, J. E. Pearson, Y. Tserkovnyak, K. L. Wang, O. Heinonen, S. G. E. te Velthuis, and A. Hoffmann, Blowing magnetic skyrmion bubbles, Science **349**, 283 (2015).

[10] W. Jiang, G. Chen, K. Liu, J. Zang, S. G. te Velthuis, and A. Hoffmann, Skyrmions in magnetic multilayers, Phys. Rep. **704**, 1 (2017).

[11] J. Matsuno, N. Ogawa, K. Yasuda, F. Kagawa, W. Koshibae, N. Nagaosa, Y. Tokura, and M. Kawasaki, Interface-driven topological Hall effect in $SrRuO_3$-$SrIrO_3$ bilayer, Sci. Adv. **2**, e1600304 (2016).

[12] K.-Y. Meng, A. S. Ahmed, M. Baćani, A.-O. Mandru, X. Zhao, N. Bagués, B. D. Esser, J. Flores, D. W. McComb, H. J. Hug, and F. Y. Yang, Observation of nanoscale skyrmions in $SrIrO_3/SrRuO_3$ bilayers, Nano Lett. **19**, 3169 (2019).

[13] A. Fert, N. Reyren, and V. Cros, Magnetic skyrmions: Advances in physics and potential applications, Nat. Rev. Mater. **2**, 17031 (2017).

[14] X. Yu, J. P. DeGrave, Y. Hara, T. Hara, S. Jin, and Y. Tokura, Observation of the magnetic skyrmion lattice in a mnsi nanowire by Lorentz TEM, Nano Lett. **13**, 3755 (2013).

[15] S. Heinze, K. Von Bergmann, M. Menzel, J. Brede, A. Kubetzka, R. Wiesendanger, G. Bihlmayer, and S. Blügel, Spontaneous atomic-scale magnetic skyrmion lattice in two dimensions, Nat. Phys. **7**, 713 (2011).

[16] O. Boulle, J. Vogel, H. Yang, S. Pizzini, D. de Souza Chaves, A. Locatelli, T. O. Menteş, A. Sala, L. D. Buda-Prejbeanu, O. Klein, M. Belmeguenai, Y. Roussignéa, A. Stashkevich, S. M. Chérif, L. Aballe, M. Foerster, M. Chshiev, S. Auffret, I. M. Miron, and G. Gaudin, Room-temperature chiral magnetic skyrmions in ultrathin magnetic nanostructures, Nat. Nanotechnol. **11**, 449 (2016).

[17] G. Chen, A. Mascaraque, A. T. N'Diaye, and A. K. Schmid, Room temperature skyrmion ground state stabilized through interlayer exchange coupling, Appl. Phys. Lett. **106**, 242404 (2015).

[18] S. Mühlbauer, B. Binz, F. Jonietz, C. Pfleiderer, A. Rosch, A. Neubauer, R. Georgii, and P. Böni, Skyrmion lattice in a chiral magnet, Science **323**, 915 (2009).

[19] Y. Yamasaki, D. Morikawa, T. Honda, H. Nakao, Y. Murakami, N. Kanazawa, M. Kawasaki, T. Arima, and Y. Tokura,

Dynamical process of skyrmion-helical magnetic transformation of the chiral-lattice magnet FeGe probed by small-angle resonant soft x-ray scattering, Phys. Rev. B **92**, 220421(R) (2015).

[20] H. Huang, S.-J. Lee, B. Kim, B. Sohn, C. Kim, C.-C. Kao, and J.-S. Lee, Detection of the chiral spin structure in ferromagnetic $SrRuO_3$ thin film, ACS Appl. Mater. Interfaces **12**, 37757 (2020).

[21] P. Zhang, A. Das, E. Barts, M. Azhar, L. Si, K. Held, M. Mostovoy, and T. Banerjee, Robust skyrmion-bubble textures in $SrRuO_3$ thin films stabilized by magnetic anisotropy, Phys. Rev. Research **2**, 032026(R) (2020).

[22] C. Wang, C.-H. Chang, A. Herklotz, C. Chen, F. Ganss, U. Kentsch, D. Chen, X. Gao, Y.-J. Zeng, O. Hellwig, M. Helm, S. Gemming, Y.-H. Chu, and S. Q. Zhou, Topological Hall effect in single thick $SrRuO_3$ layers induced by defect engineering, Adv. Electron. Mater. **6**, 2000184 (2020).

[23] B. Pang, L. Zhang, Y. Chen, J. Zhou, S. Yao, S. Zhang, and Y. Chen, Spin-glass-like behavior and topological Hall effect in $SrRuO_3/SrIrO_3$ superlattices for oxide spintronics applications, ACS Appl. Mater. Interfaces **9**, 3201 (2017).

[24] L. F. Wang, Q. Y. Feng, Y. Kim, R. Kim, K. H. Lee, S. D. Pollard, Y. J. Shin, H. B. Zhou, W. Peng, D. Lee, W. J. Meng, H. Yang, J. H. Han, M. Kim, Q. Y. Lu, and T. W. Noh, Ferroelectrically tunable magnetic skyrmions in ultrathin oxide heterostructures, Nat. Mater. **17**, 1087 (2018).

[25] Y. Ohuchi, J. Matsuno, N. Ogawa, Y. Kozuka, M. Uchida, Y. Tokura, and M. Kawasaki, Electric-field control of anomalous and topological Hall effects in oxide bilayer thin films, Nat. Commun. **9**, 213 (2018).

[26] Y. Gu, Y.-W. Wei, K. Xu, H. Zhang, F. Wang, F. Li, M. S. Saleem, C.-Z. Chang, J. Sun, C. Song *et al.*, Interfacial oxygen-octahedral-tilting-driven electrically tunable topological Hall effect in ultrathin $SrRuO_3$ films, J. Phys. D **52**, 404001 (2019).

[27] Q. Qin, L. Liu, W. Lin, X. Shu, Q. Xie, Z. Lim, C. Li, S. He, G. M. Chow, and J. Chen, Emergence of topological Hall effect in a $SrRuO_3$ single layer, Adv. Mater. **31**, 1807008 (2019).

[28] D. Kan and Y. Shimakawa, Defect-induced anomalous transverse resistivity in an itinerant ferromagnetic oxide, Phys. Status Solidi (b) **255**, 1800175 (2018).

[29] L. Wang, Q. Feng, H. G. Lee, E. K. Ko, Q. Lu, and T. W. Noh, Controllable thickness inhomogeneity and berry curvature engineering of anomalous Hall effect in $SrRuO_3$ ultrathin films, Nano Lett. **20**, 2468 (2020).

[30] P.-C. Wu, H. Song, Y. Yuan, B. Feng, Y. Ikuhara, R. Huang, P. Yu, C.-G. Duan, and Y.-H. Chu, Thickness dependence of transport behaviors in $SrRuO_3/SrTiO_3$ superlattices, Phys. Rev. Materials **4**, 014401 (2020).

[31] G. Kimbell, P. M. Sass, B. Woltjes, E. K. Ko, T. W. Noh, W. Wu, and J. W. Robinson, Two-channel anomalous Hall effect in $SrRuO_3$, Phys. Rev. Materials **4**, 054414 (2020).

[32] M. Ziese, L. Jin, and I. Lindfors-Vrejoiu, Unconventional anomalous Hall effect driven by oxygen-octahedra-tailoring of the $SrRuO_3$ structure, J. Phys.: Mater. **2**, 034008 (2019).

[33] D. J. Groenendijk, C. Autieri, T. C. van Thiel, W. Brzezicki, J. R. Hortensius, D. Afanasiev, N. Gauquelin, P. Barone, K. H. W. van den Bos, S. van Aert, J. Verbeeck, A. Filippetti, S. Picozzi, M. Cuoco, and A. D. Caviglia, Berry phase engineering at oxide interfaces, Phys. Rev. Research **2**, 023404 (2020).

[34] N. Mohanta, E. Dagotto, and S. Okamoto, Topological Hall effect and emergent skyrmion crystal at manganite-iridate oxide interfaces, Phys. Rev. B **100**, 064429 (2019).

[35] L. Wysocki, J. Schöpf, M. Ziese, L. Yang, A. Kovács, L. Jin, R. B. Versteeg, A. Bliesener, F. Gunkel, L. Kornblum, R. Dittmann, P. H. M. van Loosdrecht, and I. Lindfors-Vrejoiu, Electronic inhomogeneity influence on the anomalous Hall resistivity loops of $SrRuO_3$ epitaxially interfaced with 5*d* perovskites, ACS Omega **5**, 5824 (2020).

[36] L. Wysocki, R. Mirzaaghayev, M. Ziese, L. Yang, J. Schöpf, R. B. Versteeg, A. Bliesener, J. Engelmayer, A. Kovács, L. Jin, F. Gunkel, R. Dittmann, P. H. M. van Loosdrecht, and I. Lindfors-Vrejoiu, Magnetic coupling of ferromagnetic $SrRuO_3$ epitaxial layers separated by ultrathin nonmagnetic $SrZrO_3/SrIrO_3$, Appl. Phys. Lett. **113**, 192402 (2018).

[37] L. Bergmann, P. Düring, S. Agrestini, A. Efimenko, S.-C. Liao, Z. Hu, P. Gargiani, C.-J. Choi, H. Baik, D.-S. Park, K. Dörr, and A. D. Rata, Growth-sequence-dependent interface magnetism of $SrIrO_3$-$La_{0.7}S_{0.3}MnO_3$ bilayers, AIP Adv. **10**, 035132 (2020).

[38] L. Wysocki, L. Yang, F. Gunkel, R. Dittmann, P. H. van Loosdrecht, and I. Lindfors-Vrejoiu, Validity of magnetotransport detection of skyrmions in epitaxial $SrRuO_3$ heterostructures, Phys. Rev. Materials **4**, 054402 (2020).

[39] K. Samanta, M. Ležaić, M. Merte, F. Freimuth, S. Blügel, and Y. Mokrousov, Crystal Hall and crystal magneto-optical effect in thin films of $SrRuO_3$, J. Appl. Phys. **127**, 213904 (2020).

[40] See Supplemental Material at http://link.aps.org/supplemental/10.1103/PhysRevMaterials.5.014403 for more information on the sample fabrication and on the microstructure of the multilayer with $m = 6$, for AHE loops and MOKE loops data of a second trilayer and a multilayer with $m = 3$, and of an asymmetric $SrIrO_3/SrRuO_3$ bilayer, all made with the PLD system at University of Cologne.

[41] K. Momma and F. Izumi, Vesta 3 for three-dimensional visualization of crystal, volumetric and morphology data, J. Appl. Crystallogr. **44**, 1272 (2011).

[42] Y. J. Chang, C. H. Kim, S.-H. Phark, Y. Kim, J. Yu, and T. Noh, Fundamental Thickness Limit of Itinerant Ferromagnetic $SrRuO_3$ Thin Films, Phys. Rev. Lett. **103**, 057201 (2009).

[43] Z. T. Zeng, J. T. Feng, X. Zheng, C. H. Wang, J. W. Liu, Z. X. Lu, F.-X. Jiang, X.-H. Xu, Z. M. Wang, and R.-W. Li, Emergent ferromagnetism with tunable perpendicular magnetic anisotropy in short-periodic $SrIrO_3/SrRuO_3$ superlattices, Appl. Phys. Lett. **116**, 142401 (2020).

[44] Y. J. Zhang, Y. Z. Luo, L. Wu, M. Suzuki, Q. H. Zhang, Y. Hirata, K. Yamagami, K. Takubo, K. Ikeda, K. Yamamoto, A. Yasui, N. Kawamura, C. Lin, K. Koshiishi, X. Liu, J. X. Zhang, Y. Hotta, R. Wang, A. Fujimori, Y. H. Lin, C. W. Nan, L. Shen, and H. Wadat, Interfacial-hybridization-modified ir ferromagnetism and electronic structure in $LaMnO_3/SrIrO_3$ superlattices, Phys. Rev. Research **2**, 033496 (2020).

[45] S. L. Zhang, Y. Liu, L. J. Collins-McIntyre, T. Hesjedal, J. Y. Zhang, S. G. Wang, and G. H. Yu, Extraordinary hall balance, Sci. Rep. **3**, 2087 (2013).

[46] Z. Fang, N. Nagaosa, K. S. Takahashi, A. Asamitsu, R. Mathieu, T. Ogasawara, H. Yamada, M. Kawasaki, Y. Tokura, and K. Terakura, The anomalous Hall effect and magnetic monopoles in momentum space, Science **302**, 92 (2003).

[47] N. Haham, Y. Shperber, M. Schultz, N. Naftalis, E. Shimshoni, J. W. Reiner, and L. Klein, Scaling of the anomalous Hall effect in $SrRuO_3$, Phys. Rev. B **84**, 174439 (2011).

[48] I. Lindfors-Vrejoiu and M. Ziese, Topological Hall effect in antiferromagnetically coupled $SrRuO_3/La_{0.7}S_{0.3}MnO_3$ epitaxial heterostructures, Phys. Status Solidi (b) **254**, 1600556 (2017).

[49] G. Malsch, D. Ivaneyko, P. Milde, L. Wysocki, L. Yang, P. H. van Loosdrecht, I. Lindfors-Vrejoiu, and L. M. Eng, Correlating the nanoscale structural, magnetic, and magneto-transport properties in $SrRuO_3$-based perovskite thin films: Implications for oxide skyrmion devices, ACS Appl. Nano Mater. **3**, 1182 (2020).

[50] X. J. Wang, D. Vanderbilt, J. R. Yates, and I. Souza, Fermi-surface calculation of the anomalous Hall conductivity, Phys. Rev. B **76**, 195109 (2007).

[51] Y. Chen, D. L. Bergman, and A. A. Burkov, Weyl fermions and the anomalous Hall effect in metallic ferromagnets, Phys. Rev. B **88**, 125110 (2013).

[52] D. Vanderbilt, I. Souza, and F. D. M. Haldane, Comment on "weyl fermions and the anomalous Hall effect in metallic ferromagnets," Phys. Rev. B **89**, 117101 (2014).

[53] B. Sohn, E. Lee, W. Kyung, M. Kim, H. Ryu, J. S. Oh, D. Kim, J. K. Jung, B. Kim, M. Han *et al.*, Sign-tunable anomalous Hall effect induced by symmetry-protected nodal structures in ferromagnetic perovskite oxide thin films, arXiv:1912.04757.

[54] A. Gerber, Interpretation of experimental evidence of the topological Hall effect, Phys. Rev. B **98**, 214440 (2018).

[55] D. Kan, T. Moriyama, K. Kobayashi, and Y. Shimakawa, Alternative to the topological interpretation of the transverse resistivity anomalies in $SrRuO_3$, Phys. Rev. B **98**, 180408(R) (2018).

[56] X. Ma, G. Yu, C. Tang, X. Li, C. He, J. Shi, K. L. Wang, and X. Li, Interfacial Dzyaloshinskii-Moriya Interaction: Effect of 5*d* Band Filling and Correlation with Spin Mixing Conductance, Phys. Rev. Lett. **120**, 157204 (2018).

[57] M. Belmeguenai, M. S. Gabor, Y. Roussigné, T. Petrisor, R. B. Mos, A. Stashkevich, S. M. Chérif, and C. Tiusan, Interfacial dzyaloshinskii-moriya interaction sign in Ir/Co_2FeAl systems investigated by brillouin light scattering, Phys. Rev. B **97**, 054425 (2018).